J. Phys. B: At. Mol. Opt. Phys. **32** (1999) 81–94. Printed in the UK PII: S0953-4075(99)95605-5

A theoretical study of mutual neutralization in $Li^+ + H^-$ collisions

H Croft†§, A S Dickinson† and F X Gadéa‡

† Department of Physics, The University of Newcastle upon Tyne, Newcastle upon Tyne NE1 7RU, UK

‡ Laboratoire de Physique Quantique, IRSAMC, Université Paul Sabatier, 118 Route de Narbonne, F-31062 Toulouse Cedex, France

Received 7 July 1998

Abstract. First principles calculations of mutual neutralization in $Li^+ + H^-$ and $Li^+ + D^-$ collisions have been performed for low energies (0.68–50.0 eV). A diabatic representation is used for eight $^1\Sigma^+$ electronic states determined directly within an *ab initio* calculation. For the comparison with the recent merged-beam experiment the finite acceptance angle of the detector has been taken into account. An improved ionic diabatic curve, corrected for deficiencies in the *ab initio* electron affinity of H, has also been used. The large cross section at low energy for this mutual neutralization is due predominantly to the almost optimal efficiency for the non-adiabatic transition to the neutral Li(3s)H(1s) state. The calculated cross section exceeds experiment by no more than about 20%, indicating that the neutral–ionic diabatic crossings and couplings are accurately evaluated by the *ab initio* approach.

1. Introduction

Mutual neutralization of oppositely charged ions is of interest in cool plasmas. For the prototype $H^+ + H^-$ reaction, generally good agreement has been obtained between experiment (Szücs *et al* 1984, Peart and Hayton 1992) and theory (Fussen and Kubach 1986) below 20 eV. In this case the degeneracy of the H(nl) levels introduces unique features absent for other ions. The reaction

$$Li^+ + H^- \rightarrow Li + H \tag{1}$$

(or its deuterium analogue) is among the simplest mutual neutralization reactions as it involves the closed-shell Li^+ ion and hence is accessible to relatively sophisticated theoretical calculations. Values of the rate coefficient for this reaction are employed in modelling the lithium chemistry of the early universe (Stancil *et al* 1996 and references therein).

Absolute cross sections for reaction (1) have been measured in an inclined-beam experiment by Peart and Foster (1987) for collision energies above 30 eV and more recently by Peart and Hayton (1994) with merged beams at energies down to 0.68 eV. Early theoretical studies within the Landau–Zener framework were performed by Bates and Boyd (1956). These studies have been refined by Janev and Radulović (1978), who estimated the non-adiabatic couplings using an asymptotic method and employed the Landau–Zener approximation with some corrections. Model potential and *ab initio* methods to determine the potentials and couplings were performed by Méndez *et al* (1990) to calculate cross sections at energies

§ Present address: British Airways, Newcastle upon Tyne, UK.

0953-4075/99/010081+14$19.50

above 25 eV. A single-active electron atomic expansion was employed by Ermolaev (1992) for energies above 100 eV. Lin *et al* (1996) employed, at a collision energy of 375 eV, a procedure similar to that of Ermolaev and then extrapolated to lower energies assuming the same transition probabilities but allowing for Coulomb focusing effects. This very simple procedure gives good agreement with experiment above about 50 eV and at 0.7 eV, but significantly underestimates the cross section between these energies.

Here we extend previous molecular-expansion calculations to the lower energies investigated in the recent merged-beam experiments (Peart and Hayton 1994). These low-energy measurements probe distant crossings and hence are particularly sensitive to the accuracy of the molecular structure calculations at long range—a region not readily accessible to spectroscopy. These measurements were performed replacing H^- by D^-, since this offered experimental advantages, and so we have considered both H^- and D^- neutralization. Except at low energies, say below about 20 eV, the total cross section is a function only of the speed of the H^- or the D^- ion and hence cross sections for one isotope can readily be scaled for the other. However, at low energies where trajectory effects, particularly Coulomb focusing, are important, the cross section is not simply a function of the relative velocity and no scaling is reliable. At these low energies a fully quantal description of the relative motion is desirable.

In any beam experiment the maximum angle of scattering of each of the beams in the laboratory is determined purely by kinematic factors. If the detectors employed subtend less than this maximum scattering angle then consideration has to be given to that part of the differential cross section not detected. We shall see below that this must be allowed for in these experiments, where at low energies the Coulomb forces generate relatively wide-angle scattering.

We have employed the molecular potentials and couplings of Boutalib and Gadéa (1992), together with some improvements to give a better description of the ionic channel. We have included eight molecular states of $^1\Sigma^+$ symmetry in our description of the process: the ionic entrance channel and seven neutral exit channels dissociating to Li(nl) + H(1s), with $nl = 2s$, 2p, 3s, 3p, 3d, 4s and 4p. In the absence of significant radial couplings, rotational couplings can be the primary charge-transfer mechanism. However, such conditions do not apply here so rotational couplings have not been included, although they would undoubtedly affect the magnetic substate distributions in the final channels. The molecular wavefunctions employed here have also been used to calculate dipole moments (Berriche and Gadéa 1995) and non-radiative lifetimes in the $A\,^1\Sigma^+$ state (Gadéa *et al* 1997).

In the following section we briefly review the molecular expansion method and the resulting coupled equations for the radial motion. The adiabatic potentials and non-adiabatic couplings are considered in section 3. Total cross section results are discussed in section 4, whilst differential cross sections and partial cross sections are examined in section 5. A summary and conclusions are given in section 6.

2. Molecular expansion method

While the molecular expansion method (Macias and Riera 1982, Kimura and Lane 1990) is conventionally described in an adiabatic basis, here we have used a diabatic description. The *ab initio* calculations employed here were diabatic and results in an adiabatic basis were derived from these for spectroscopic applications and for comparison with previous work.

The total wavefunction $\Psi(\boldsymbol{r}, \boldsymbol{R})$ is expanded in a diabatic molecular electronic basis $\{\phi_n(\boldsymbol{r}, R)\}$, where $\boldsymbol{r}$ is a collective coordinate for the electrons and $\boldsymbol{R}$ denotes the relative

position of the nuclei:

$$\Psi(\boldsymbol{r}, \boldsymbol{R}) = \sum_{n=1}^{8} F_n(\boldsymbol{R})\phi_n(\boldsymbol{r}, R). \tag{2}$$

Here the sum runs over the ionic entrance channel and the seven neutral channels of $^1\Sigma^+$ symmetry discussed above. In view of the low speeds of interest here we have not included an electron translation factor, as in the work of Fussen and Kubach (1986) on $H^+ + H^-$.

The resulting radial coupled equations for orbital angular momentum l are given in matrix notation

$$\frac{\mathrm{d}^2}{\mathrm{d}R^2}\boldsymbol{F}^l + \frac{2\mu}{\hbar^2}\left[\left(\mathcal{E} - \frac{l(l+1)}{R^2}\right)\mathbf{I} - \mathbf{V}\right]\boldsymbol{F}^l = 0 \tag{3}$$

μ being the reduced mass, $\mathcal{E}$ the total energy and $\mathbf{V}$ the diabatic potential matrix. The numerical solution employed the Manoloupolos (1986) improved version of Johnson's (1973) log-derivative algorithm.

Differential cross sections (to be discussed further in section 5) were calculated from the scattering amplitude f_{ij}, between the ionic entrance channel i and the final neutral channel j, using

$$f_{ij}(\theta) = \frac{1}{2\mathrm{i}k}\sum_l (2l+1)T_{ij}^l P_l(\cos\theta) \tag{4}$$

where k denotes the wavenumber, T_{ij}^l is the corresponding transition matrix element for orbital angular-momentum quantum number l and $P_l(x)$ is the Legendre polynomial of order l.

In the next section we review the calculations of the diabatic potential matrix.

3. *Ab initio* potentials and couplings

Nearly all the $^1\Sigma^+$ electronic states below the ionic asymptote (Li^+H^-) are involved in the present calculation, i.e. Li(2s, 2p, 3s, 3p, 3d, 4s, 4p)H(1s). Hence the eight diabatic states have been determined for a broad range of internuclear distances from 1.8 to 243 a_0 according to the approach described in Boutalib and Gadéa (1992). The *ab initio* calculation uses a pseudo-potential for the Li core and an operatorial l-dependent approach for estimating the important core–valence correlation. It relies on a diabatization procedure which combines variational effective Hamiltonian theory (Gadéa 1991) with an effective metric for the overlap between the atomic basis sets (Gadéa and Pelissier 1990). In the diabatic representation we have potential coupling instead of the radial coupling arising from the adiabatic representation.

For completeness we report in figures 1 and 2 the adiabatic and diabatic potential curves, respectively. The ionic curve imprints these potentials and crosses the other diabatic curves at increasing interatomic distances. For the $n = 3$ curves, which will play the major role in the neutralization, the diabatic crossings occur at 20.9, 31.7 and 33.7 a_0 for 3s, 3p and 3d, respectively, consistent with the observed large neutralization cross section (Peart and Hayton 1994). Radial couplings computed assuming a strictly diabatic representation were reported by Gadéa and Boutalib (1993) and compared favourably with direct *ab initio* calculations (Méndez *et al* 1990), giving confidence in the *ab initio* diabatization method.

Comparison of these results, which we term the original data, with spectroscopic data has been reviewed by Boutalib and Gadéa (1992). When the ionic diabatic curve is corrected for the small ($\sim$420 cm^{-1}) underestimate in the hydrogen electron affinity the values for the binding energies of the X and A electronic states agree remarkably well with experiment: within 0.7%. It was also shown there that this electron affinity error is the main source of

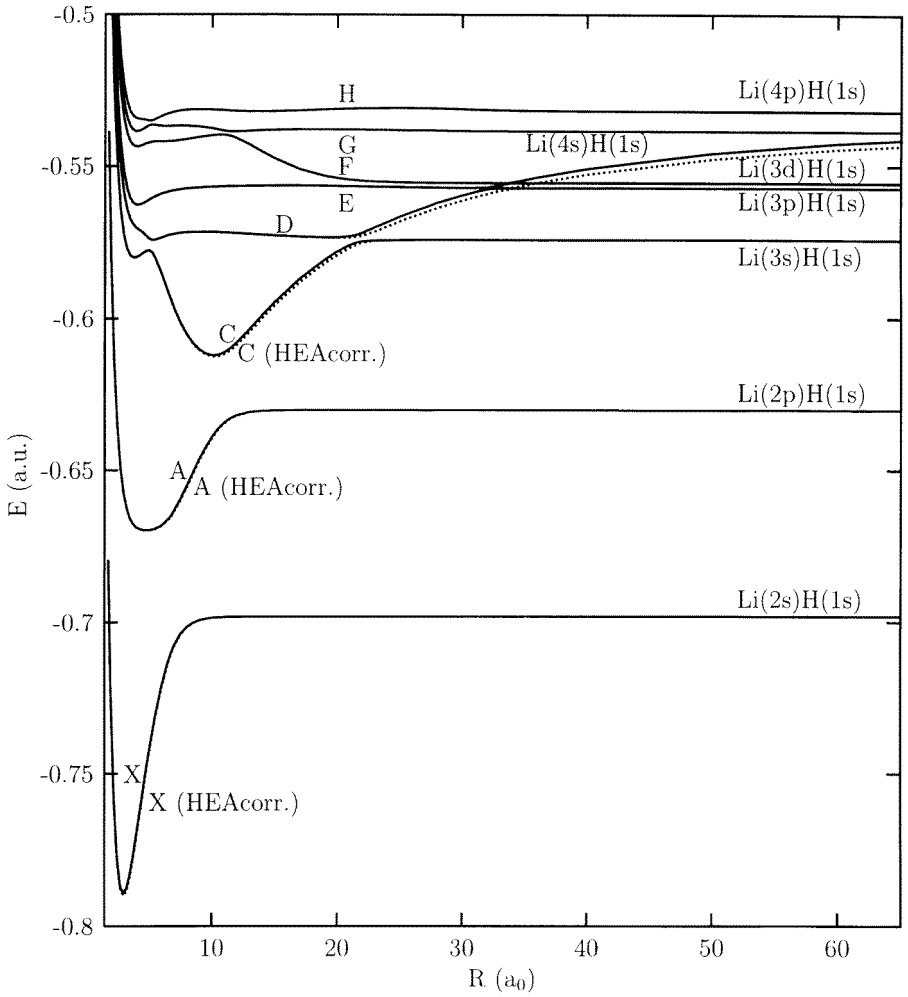

Figure 1. LiH adiabatic potential curves for the lowest eight $^1\Sigma^+$ states of LiH: full curves, *ab initio* result; dotted curves, using the improved ionic curve (with the corrected electron affinity of H).

the discrepancies in the *ab initio* calculation, since the theoretical results with and without the correction bracket all the observed vibrational spacings for the A state: the spacings were too large for the original *ab initio* potentials and slightly too small when the constant asymptotic correction is introduced. For the A state, the improvement broadens the well and leads to a systematic decrease in the vibrational spacings. Potentials and couplings using this correction are termed the improved results.

When the ionic curve is improved the crossings with the neutral curves are shifted to larger distances. While performing this correction we change only the ionic diagonal matrix element of the diabatic Hamiltonian. With the R-dependent correction, which accounts for basis-set superposition error (the basis around the H atom is improved by the Li basis set), the crossings for the $n = 3$ series are now at 21.5, 33.9 and 35.9 a_0 for 3s, 3p and 3d, respectively. Since the corresponding neutral–ionic diabatic couplings decrease exponentially with separation, the couplings are weaker with the improved ionic curve. In the following sections results

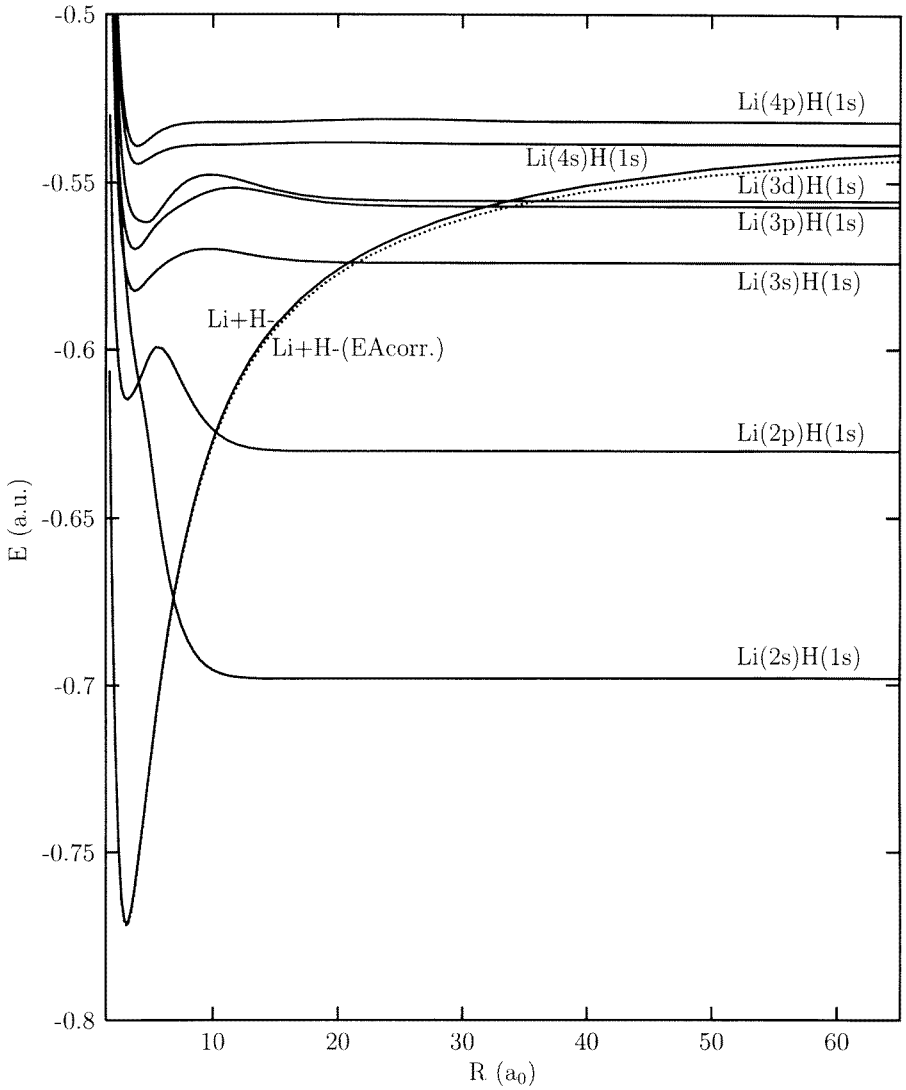

Figure 2. Diabatic potential energy curves for LiH: full curves, *ab initio* result; dotted curve, improved ionic curve (only this curve is modified in the diabatic representation).

for neutralization with and without this R-dependent correction will be discussed, since their differences give some insight into the sensitivity of the neutralization cross section to the potentials and couplings employed.

4. Total cross section results

Results calculated using the original diabatic potential matrix for total cross sections for H^- and D^- neutralization are presented in figures 3 and 4, respectively, for energies between 0.68 eV and 20 eV for H^-, 0.68 eV and 32 eV for D^-. Also shown are the cumulative results for neutralization into the lithium 3s, 3p and 3d channels. Note that the cumulative 3d result is barely distinguishable from that for the total cross section. Of the other channels

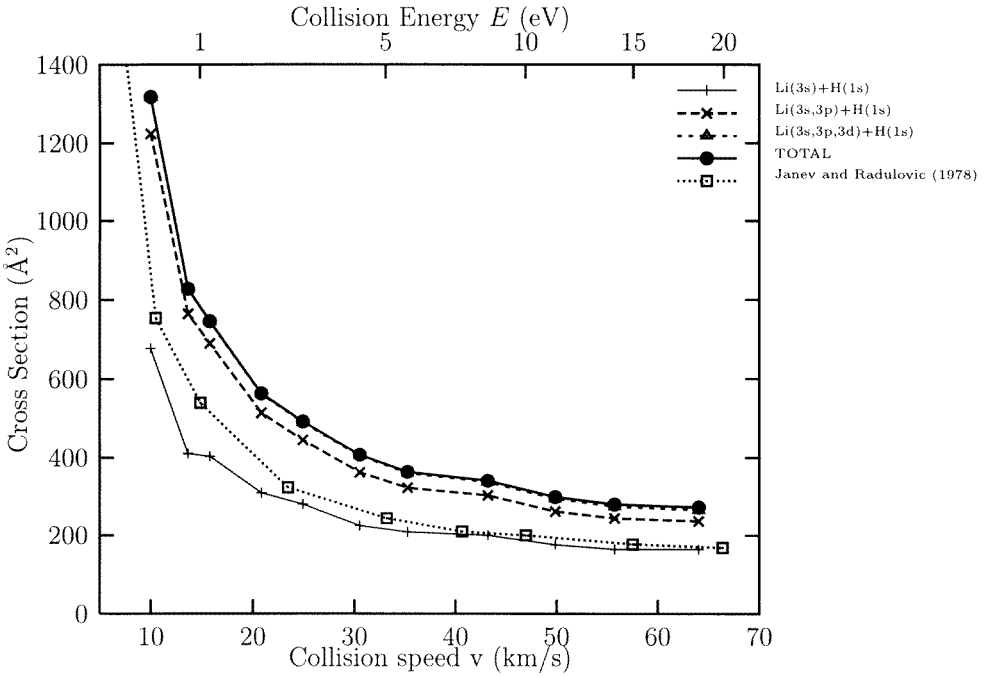

Figure 3. Neutralization cross sections with the original potentials for the $Li^+ + H^-$ collision.

(2s, 2p, 4s, 4p) the most important is the 2p, which contributes less than 2% at all energies considered. For the 2s and 2p channels the electronic couplings with the ionic channel are large and we have almost adiabatic behaviour, while for the 4s and 4p channels the couplings are very small and almost diabatic behaviour is observed: hence both cases contribute little to the neutralization. The cumulative plots clearly show the neutralizations to be dominated by transitions to the Li(3s, 3p) + H/D(1s) channels, with the 3p contributions rivalling the 3s at the lowest energies.

To assess the importance of focusing we compare the H^- and D^- cross sections as a function of speed in figure 5. It is clear that in this system focusing becomes negligible above about 20 eV amu^{-1}. Such behaviour can be understood in terms of the relation between the classical impact parameter b and the pseudo-crossing distance R_c, in the presence of a focusing potential $V(R)$ in the entrance channel: at collision energy E, $b^2 = R_c^2(1 - V(R_C)/E)$. For the more important 3s pseudo-crossing $V(R_C)$ is about 1.25 eV, so the focusing effect is below 10% by about 20 eV.

The results of Janev and Radulović (1978) for H^- are also presented in figure 3. Generally their values are about 30% smaller than those obtained here.

Results for D^- are compared in figure 6 with the measurements of Peart and Hayton (1994). While our calculated cross section shows a similar energy dependence to the measurements, its magnitude is significantly larger. At the lowest energy, 0.68 eV, the calculated value is about twice the measured value and the fractional difference falls to about 33% at 20 eV, before rising again to about 50% at the highest energy, 33 eV.

This prompted a two-fold attempt to understand the differences. First, the calculated potentials and couplings involving the ionic channel were improved, as discussed in section 3. Results with these new potentials and couplings are also shown in figure 6 and are listed in table 1. Values for D^- with the original potentials are 20–25% larger than those obtained with

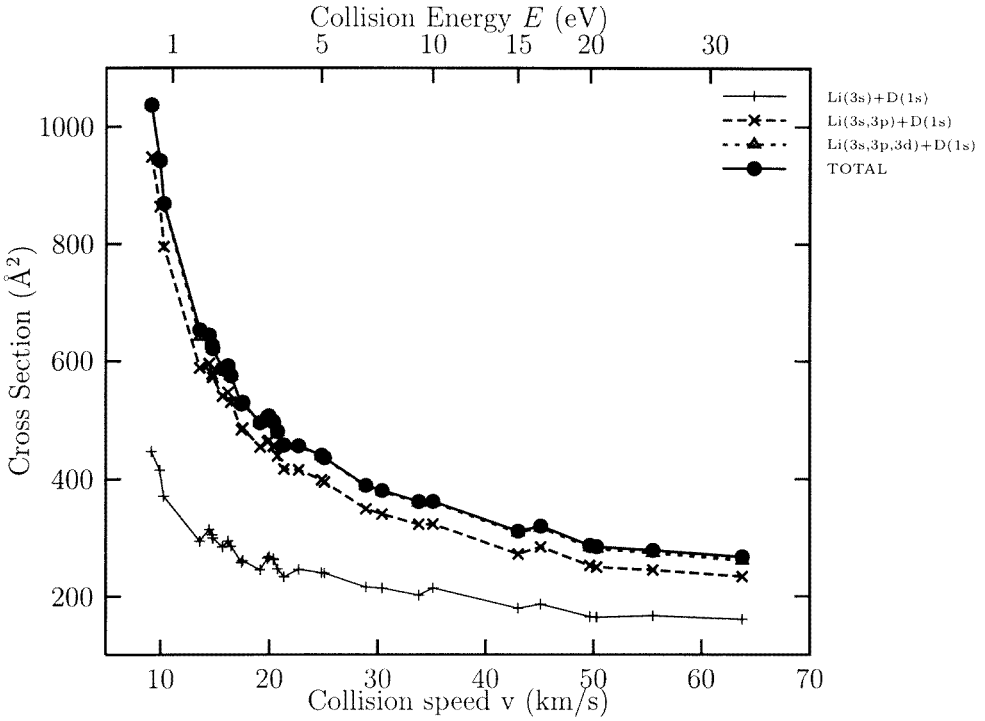

Figure 4. Neutralization cross sections with the original potentials for the $Li^+ + D^-$ collision.

Table 1. Cross sections, in Å^2, for $Li^+ + D^- \longrightarrow Li(1s^2nl) + D(1s)$.

	nl						
E (eV)	2s	2p	3s	3p	3d	4s	4p
0.68	0.0008	0.016	539.5	317.5	32.0	0.046	0.0031
0.86	0.040	0.026	436.8	267.4	26.5	0.023	0.0020
1.50	0.036	0.089	353.2	190.8	18.6	0.067	0.011
2.47	0.007	0.087	307.7	144.4	15.5	0.24	0.027
3.37	0.078	0.122	261.9	120.9	14.5	0.305	0.052
5.11	0.030	0.205	233.9	98.5	15.8	0.457	0.126
6.78	0.035	0.291	237.5	83.2	15.3	0.512	0.110
9.27	0.010	0.550	206.9	75.1	18.8	0.589	0.172
16.5	0.011	1.63	175.1	60.0	15.6	0.737	0.162
25.0	0.0097	3.28	164.1	50.3	15.8	0.776	0.227
33.0	0.022	4.81	147.9	47.8	14.3	0.822	0.434
50.1	0.084	8.96	128.6	38.5	16.2	0.433	1.09

the improved potentials, while for H^- the new results are 20–25% larger than those of Janev and Radulović (1978).

It can be seen that the agreement with experiment is better but significant discrepancies remain. The error remains largest, 75%, at the lowest energy but drops to 35% by 1.5 eV and reaches about 20% for energies above about 5 eV.

There are small-amplitude oscillations, incompletely resolved, visible in this plot. These arise from the existence of a region of stationary phase in the Stueckelberg oscillations in the

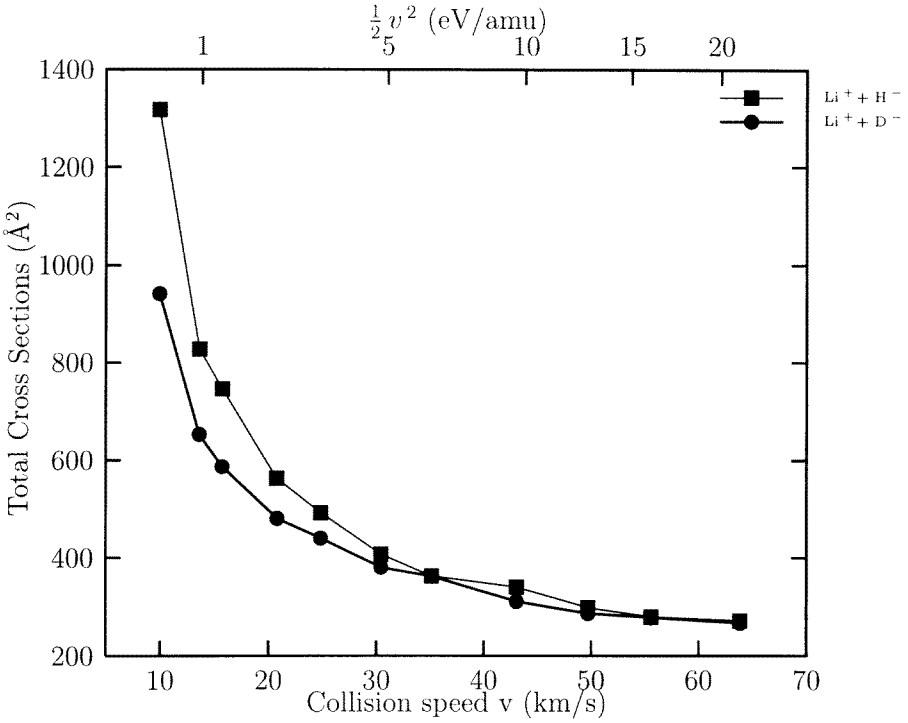

Figure 5. Comparison of the $Li^+ + H^-$ and $Li^+ + D^-$ neutralization cross sections calculated using the original potentials.

l-dependence of the transition probability.

For clarity the cumulative 3s, 3p and 3d contributions are not shown, although the 3s contribution can be found in figure 10 below. However, the 3s contribution is little altered while the 3p and 3d contributions have dropped significantly. This behaviour can be understood qualitatively in terms of a Landau–Zener analysis. The net transition probability for the 3s state is near its maximum for few-eV collisions and so is relatively insensitive to small changes in the non-adiabatic coupling parameters. For the 3p and 3d transitions, with the more distant pseudo-crossing points at 31.7 a_0 and 33.7 a_0, respectively (with the original potentials), the improved coupling is much weaker and all the energies of interest lie in the high-energy limit of the Landau–Zener model, so the cross section is proportional to the square of the coupling matrix element and inversely proportional to speed (in the absence of focusing effects).

The remaining discrepancies prompted a closer examination of the kinematics of the merged-beam experiment and this is discussed in the next section.

5. Differential cross sections

5.1. Relating laboratory and centre-of-mass angles

For the cylindrical symmetry of a merged-beam experiment, relating scattering angles in the laboratory and centre-of-mass frames is relatively straightforward. A schematic Newton diagram (Child 1974) is shown in figure 7. Here $\boldsymbol{v}$, $\boldsymbol{v}_A$, $\boldsymbol{v}_B$ denote the relative velocity and the laboratory velocities of atoms A and B, respectively, before the collision. The corresponding quantities after the collision are denoted by primes. The velocity of the centre of mass is V_{CM}.

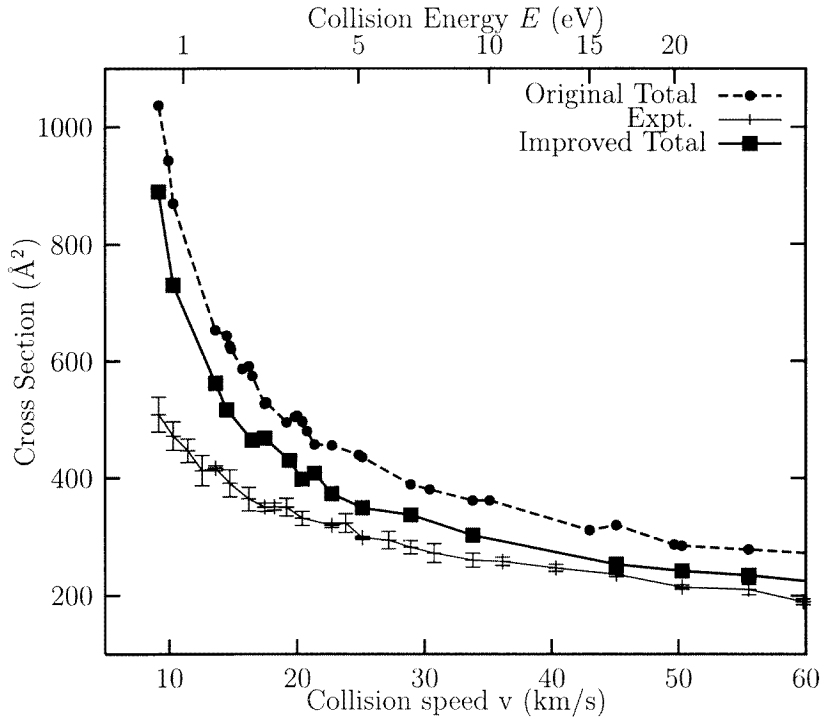

Figure 6. Comparison with experiment of $Li^+ + D^-$ results calculated using the original and improved potentials.

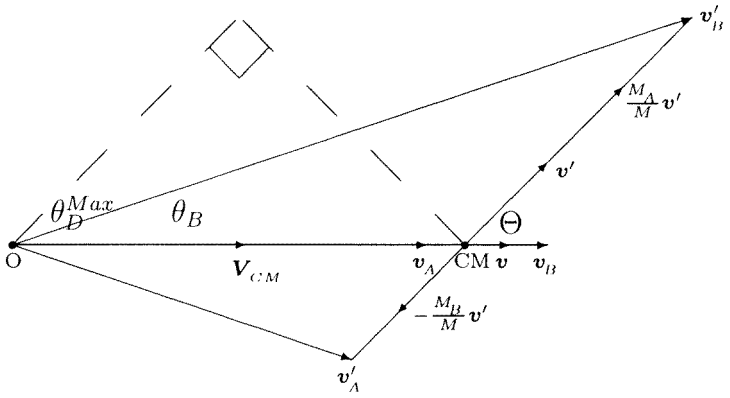

Figure 7. Relative motion in the laboratory and centre-of-mass frames.

The scattering angle in the centre-of-mass frame is denoted Θ and θ_B denotes the laboratory scattering angle of the lighter partner, B.

The experiment recorded the arrival, on the same detector, of the Li and D atoms in delayed coincidence (Peart and Hayton 1994). The detector, of diameter 2.54 cm, was placed either 82 or 108 cm from the end of the interaction region, giving upper bounds to the maximum laboratory scattering angle of 0.89° and 0.67°, respectively. Neutralization could occur anywhere within an interaction region of length 17.8 cm. Since the lighter D atoms are scattered more (see figure 7) it is sufficient to examine their detection.

Table 2. Limiting deuterium deflection angles for neutralization into the Li(3*l*) + D(1s) channels.

		$\theta_{\mathrm{D}}^{\max}$ (°)		
E (eV)	$E_{\mathrm{lab}}^{\mathrm{D}}$ (keV)	ionic—Li(3s)	ionic—Li(3p)	ionic—Li(3d)
0.68	3.08	1.3	1.1	1.1
4.19	3.2	2.2	2.1	2.1
38.9	4.72	5.1	5.0	5.0

Table 3. Limiting deflection angles detected by experiment for neutralization into the Li(3*l*)+D(1s) channels.

	ionic—Li(3s)		ionic—Li(3p)		ionic—Li(3d)	
E (eV)	Θ_- (deg)	Θ_+ (deg)	Θ_- (deg)	Θ_+ (deg)	Θ_- (deg)	Θ_+ (deg)
0.68	31.8	149.6	36.7	144.7	37.3	144.1
4.19	18.8	162.6	19.6	161.7	19.7	161.7
38.9	8.3	173.0	8.4	173.0	8.4	173.0

From the figure it can be seen that the maximum laboratory angle of deflection for the D atom, $\theta_D^{\max}$, is given by

$$\theta_D^{\max} = \arcsin\left(\frac{M_{Li}}{M}\frac{v'}{V_{CM}}\right), \tag{5}$$

where M_{Li} is the Li mass and $M = M_{Li} + M_D$ the total mass, M_D being the deuterium mass. Some values of $\theta_D^{\max}$ for the 3*l* transitions at various centre-of-mass energies and typical laboratory energies are shown in table 2.

It is straightforward to show (see figure 7) that the smaller and larger centre-of-mass scattering angles, Θ_- and Θ_+, respectively, corresponding to D scattering into laboratory angle θ_D satisfy

$$\Theta_- = \theta_D + \arcsin\left(\frac{V_{CM}\sin\theta_D}{\frac{M_{Li}}{M}v'}\right) \tag{6}$$

$$\Theta_+ = \Pi - \Theta_- + 2\theta_D. \tag{7}$$

We show in table 3 some typical values for $\Theta_\pm$ for various collision energies and laboratory D^- beam energies employed in the measurements.

5.2. Differential cross sections

The centre-of-mass differential cross section for capture into Li(3s) at a collision energy of 4.19 eV, using the original potentials, is shown in figure 8.

The extensive interference structure can be understood following the semiclassical analysis of Delvigne and Los (1973). A schematic diagram showing the two branches of the classical deflection function, $\bar{\Theta}_1(b)$ and $\bar{\Theta}_2(b)$, is shown in figure 9. These branches meet when the transition takes place at the distance of closest approach with the impact parameter b_0. The deflection angle associated with this impact parameter is, assuming Coulomb scattering,

$$\Theta_0 = \arctan\left(\frac{1}{2Eb_0}\right). \tag{8}$$

The first branch $\bar{\Theta}_1$, for which the non-adiabatic transition is made on the way out of the collision, is formed from sections d and e corresponding to attractive and repulsive neutral

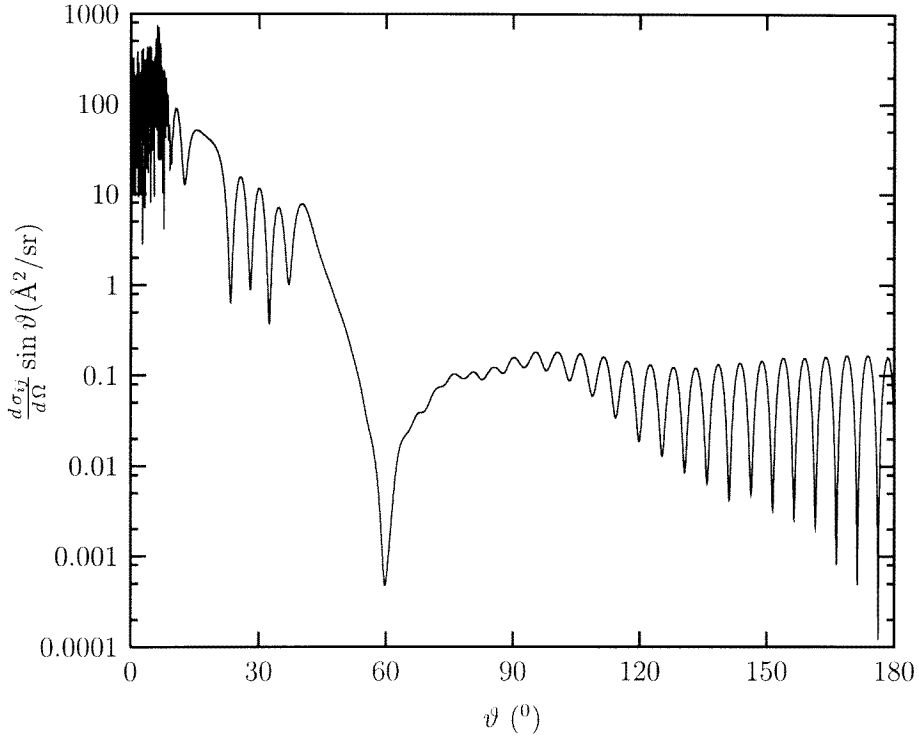

Figure 8. The ionic—Li(3s) differential cross section for $E = 4.19$ eV.

scattering, respectively. The transition is made on the way into the collision for branch $\bar{\Theta}_2$, resulting in more attractive deflection (sections b and c) than seen in the first case due to the increased exposure to the Coulomb potential. This branch exhibits a mimimum or *rainbow* angle $\Theta = -\vartheta_{\mathcal{R}}$ since the potential becomes repulsive at short range, eventually giving rise to section a of the curve.

There are essentially three regions of different oscillatory behaviour. The first region, spanning 0 to $\sim 8^\circ$, falls just beyond $\vartheta_0 = 7.5^\circ$ (see equation (7)). The corresponding parts of the typical deflection function are shown in figure 9, labelled 1, and indicate that four trajectories, two from each of the branches $\bar{\Theta}_1$ and $\bar{\Theta}_2$, contribute to the differential cross section for a given angle ϑ. The relatively large magnitude is caused by the two $\bar{\Theta}_1$ trajectories for which $\frac{\mathrm{d}\vartheta}{\mathrm{d}b}$ is small.

Figure 8 shows the interference pattern undergoing a drastic change beyond $\vartheta = 10^\circ$, with the small-angle behaviour being replaced by a series of much smaller but broader oscillations which gradually diminish until finally disappearing by $\vartheta \sim 50^\circ$. This behaviour is determined by the regions labelled 2 in figure 9, with the rainbow minimum giving rise to the last peak seen in the differential cross section at $\vartheta \sim 40^\circ$. Again four different trajectories contribute for each scattering angle ϑ, but only one of these arises from the $\bar{\Theta}_1$ branch whilst there are three from $\bar{\Theta}_2$ for the transition being made on the way into the collision. The interference pattern here is primarily the well known rainbow oscillations of potential scattering. The limiting forward scattering deflection angle $\Theta_- = 18.8^\circ$ (see table 3) is contained within this second region.

The final region, beyond the rainbow angle, is labelled 3 in figure 9. The figure shows this region to contain two entirely repulsive trajectories—one from each branch of the deflection function. The steep short-range repulsive potentials can be considered to scatter trajectories

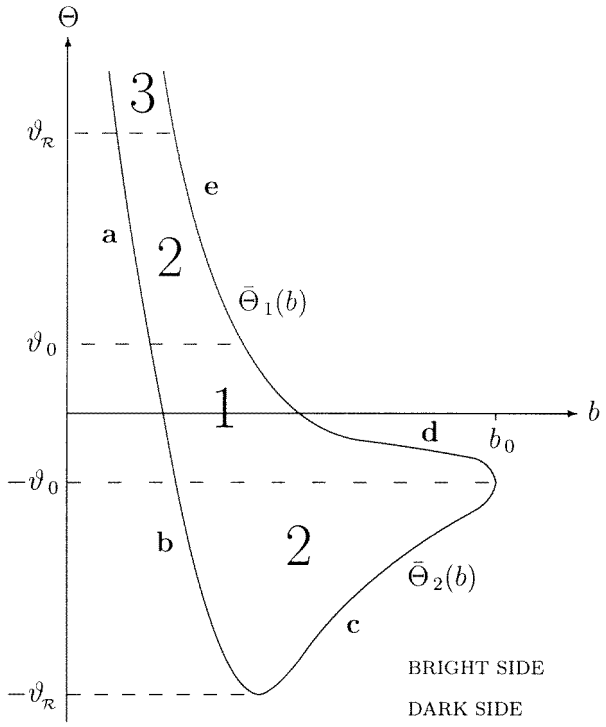

Figure 9. Typical deflection function for a mutual neutralization collision.

similarly to hard spheres, hence the maximum cross section is approximately independent of angle.

5.3. Partial cross sections

To simulate the observations of Peart and Hayton (1994) we have determined partial cross sections σ_{if}^{P} from

$$\sigma_{if}^{P} = \sigma_{if} - 2\pi \int_{\Theta_-}^{\Theta_+} \frac{\mathrm{d}\sigma_{if}}{\mathrm{d}\Omega} \sin\Theta \, \mathrm{d}\Theta. \tag{9}$$

For each energy and transition considered we have employed the values of $\Theta_{\pm}$ appropriate to the laboratory energies and angles employed. The integral has been evaluated using the trapezoidal rule with typical step sizes of 0.5°.

In figure 10 we show the results for partial and total neutralization cross sections for D^- calculated with the improved potentials and compared to the measurements of Peart and Hayton (1994). We see that the 3s partial cross section is substantially smaller ($\approx$30%) than the 3s total cross section at the lowest energy, with the difference becoming negligible above about 15 eV. For the 3p and 3d cross sections (not shown, for clarity) the effect of the finite aperture is less marked, below about 10%. Since most of these cross sections come from orbital angular momenta (impact parameters) larger than those probing the 3s pseudo-crossing, their angles of scattering are necessarily small.

The level of agreement with experiment is now much improved. Theory overestimates the cross section by about 20% at the lowest energy and is consistent with the observations for 5–25 eV, but lies somewhat above experiment for 25–50 eV.

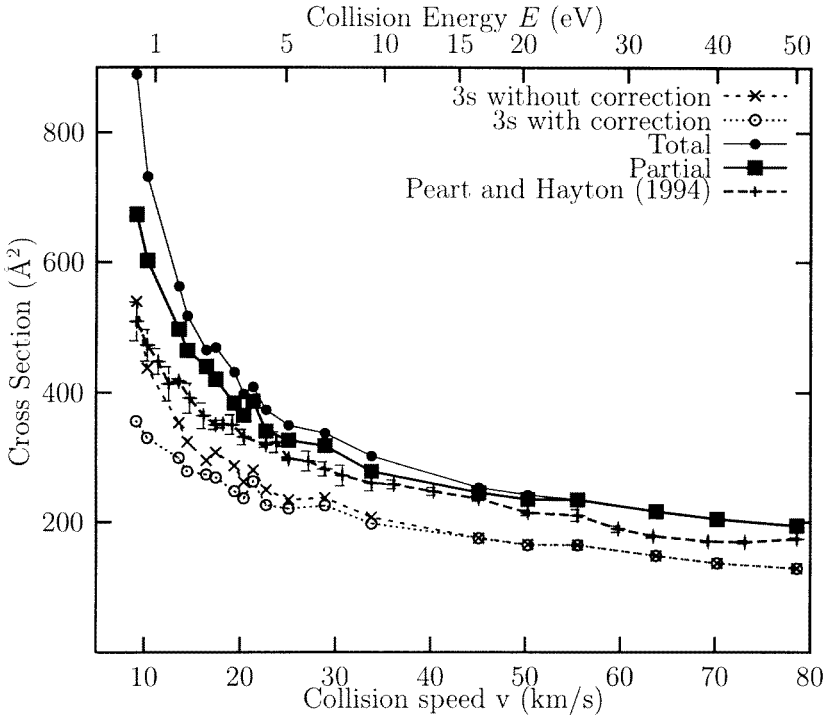

Figure 10. Comparison with experiment (Peart and Hayton 1994) of improved $Li^+ + D^-$ results, with and without finite aperture correction.

6. Summary and conclusions

We have performed *ab initio* calculations of Li^+ neutralization by H^- and D^- at collision energies between 0.68 eV and about 30 eV. Diabatic molecular expansion method potentials were calculated using a pseudopotential for the Li valence electron and the scattering problem was treated in an eight-state expansion. Some allowance has been made for the finite acceptance angle of the detector used in the measurements of Peart and Hayton (1994). The bulk of the neutralization cross section is accounted for by 3s capture with a modest contribution by 3p and, to a lesser extent, by 3d. Except at the lowest energies good agreement is obtained with these measurements.

This high efficiency of the 3s capture is consistent with the low-energy Li^+ neutralization cross section being the largest at a common velocity of those measured recently: H^+ (Peart and Hayton 1992), He^+ (Peart and Hayton 1994), H_2^+ (Peart *et al* 1997)—see figure 4 of this last reference. Also, the calculations of Janev and Radulović (1978) for the neutralization of H^- by alkali metal ions again show Li^+ having the largest cross section.

Since the 3s pseudo-crossing is traversed with nearly maximum efficiency for charge transfer it is relatively insensitive to small changes in the couplings. For the 3p and 3d contributions, on the other hand, the cross section is proportional to the square of the couplings so a small reduction in these couplings, associated with a slightly larger pseudo-crossing distance, could improve further the agreement between theory and experiment.

A change in the ionic curve in the critical crossing region by only about 320 cm^{-1}, which induces a shift of the crossings by $\sim$0.6 a_0 for the 3s pseudo-crossing and about 2 a_0 for the 3p and 3d crossings, leads to a reduction of the cross section by up to 25%. The remaining

discrepancy between the first principles calculation and the observations allows an estimate of the accuracy in the *ab initio* approach. After crudely extrapolating the previous results, the ionic curve still appears to be too high in energy by about 100 cm^{-1}. With the main asymptotic error, due to the electron affinity of the H atom, having been accounted for, the core–valence correlation estimate should now probably be improved. In that respect a systematic study of the whole series of alkali-hydrides could be helpful in establishing general trends. Work in that direction is in progress.

Measurements of the neutralization cross section are testing the long-range ionic–neutral pseudo-crossings, a region not readily accessible to spectroscopy. We note that the outer classical turning points for the highest observed vibrational levels in the X and A states are $\approx 10\, a_0$ (Stwalley and Zemke 1993). Thus the spectroscopic and collisional approaches provide complementary probes of the *ab initio* potentials and couplings. The present calculation relies on the determination of *ab initio* diabatic states and the satisfactory agreement with experiment helps confirm the reliability of the diabatization procedure used.

Acknowledgments

The work of HC and ASD was supported by EPSRC. British Council (Action Integré, 'Alliance' no 98084) support is gratefully acknowledged. We thank Dr B Peart for many valuable discussions.

References

Bates D R and Boyd T J M 1956 *Proc. Phys. Soc.* A **69** 910–6
Berriche H and Gadéa F X 1995 *Chem. Phys. Lett.* **247** 85
Boutalib A and Gadéa F X 1992 *J. Chem. Phys.* **97** 1144
Child M S 1974 *Molecular Collision Theory* (London: Academic)
Delvigne G A L and Los J 1973 *Physica* **67** 166
Ermolaev A M 1992 *J. Phys. B: At. Mol. Opt. Phys.* **25** 3133
Fussen D and Kubach C 1986 *J. Phys. B: At. Mol. Opt. Phys.* **21** L31
Gadéa F X 1991 *Phys. Rev.* A **43** 1160
Gadéa, F X, Berriche H, Roncero O, Villarreal P and Delgado Barrio G 1997 *J. Chem. Phys.* **107** 10 515
Gadéa F X and Boutalib A 1993 *J. Phys. B: At. Mol. Opt. Phys.* **26** 61
Gadéa F X and Pelissier M 1990 *J. Chem. Phys.* **93** 545
Janev R K and Radulović Z M 1978 *Phys. Rev.* A **17** 889
Johnson B R 1973 *J. Comput. Phys.* **13** 445
Kimura M and Lane N F 1990 *Adv. At. Mol. Phys.* **26** 79
Lin J T, Jiang T F and Lin C D 1996 *J. Phys. B: At. Mol. Opt. Phys.* **29** 6175
Macias A and Riera A 1982 *Phys. Rep.* **90** 299
Manoloupolos D E 1986 *J. Chem. Phys.* **85** 6425
Méndez L, Cooper I L, Dickinson A S, Mó O and Riera A 1990 *J. Phys. B: At. Mol. Opt. Phys.* **23** 2797
Peart B and Foster S J 1987 *J. Phys. B: At. Mol. Opt. Phys.* **20** L691
Peart B and Hayton D A 1992 *J. Phys. B: At. Mol. Opt. Phys.* **25** 5109–19
——1994 *J. Phys. B: At. Mol. Opt. Phys.* **27** 2551–6
Peart B, Padgett R and Hayton D A 1997 *J. Phys. B: At. Mol. Opt. Phys.* **30** 4955–61
Stancil P C, Lepp S and Dalgarno A 1996 *Astrophys. J.* **458** 401
Stwalley W C and Zemke W T 1993 *J. Phys. Chem. Ref. Data* **22** 87–112
Szücs S, Karemera M, Terao M and Brouillard F 1984 *J. Phys. B: At. Mol. Opt. Phys.* **17** 1613